frontiers in Physics

ORIGINAL RESEARCH
published: 01 April 2015
doi: 10.3389/fphy.2015.00018

Onset of fast magnetic reconnection via subcritical bifurcation

Zhibin Guo [1,2]* *and Xiaogang Wang* [1]

[1] State Key Laboratory of Nuclear Physics and Technology, School of Physics, Peking University, Beijing, China, [2] WCI Center for Fusion Theory, National Fusion Research Institute, Daejeon, South Korea

We report a phase transition model for the onset of fast magnetic reconnection. By investigating the joint dynamics of streaming instability (i.e., current driven ion acoustic in this paper) and current gradient driven whistler wave prior to the onset of fast reconnection, we show that the nonlinear evolution of current sheet (CS) can be described by a Landau-Ginzburg equation. The phase transition from slow reconnection to fast reconnection occurs at a critical thickness, $\Delta_c \simeq \frac{2}{\sqrt{\pi}}\left|\frac{v_{the}}{v_c}\right| d_e$, where v_{the} is electron thermal velocity and v_c is the velocity threshold of the streaming instability. For current driven ion acoustic, Δ_c is $\leq 10d_e$. If the thickness of the CS is narrower than Δ_c, the CS subcritically bifurcates into a rough state, which facilitates breakage of the CS, and consequently initiates fast reconnection.

Keywords: magnetic reconnections, fast reconnection, current sheets, bifurcation analysis, plasma waves

Edited by:
Valery M. Nakariakov, University of Warwick, UK

Reviewed by:
David Tsiklauri, Queen Mary University of London, UK
Valentina Zharkova, Northumbria University, UK

Correspondence:
Zhibin Guo, WCI Center for Fusion Theory, National Fusion Research Institute, Seoul National University, Room#A304, BK International House, Building 946, Gwanak-ro 1, Gwanak-gu, Seoul 151-851, South Korea
guozhipku@gmail.com

Specialty section:
This article was submitted to Stellar and Solar Physics, a section of the journal Frontiers in Physics

Received: *14 September 2014*
Accepted: *12 March 2015*
Published: *01 April 2015*

Citation:
Guo Z and Wang X (2015) Onset of fast magnetic reconnection via subcritical bifurcation. Front. Phys. 3:18. doi: 10.3389/fphy.2015.00018

1. Introduction

Critical behavior is ubiquitous in magnetic reconnection related phenomena, e.g., Ôflux transfer event at magnetopause [1, 2], solar flare, etc. A universal property in these phenomena is that there is always a long development or slow reconnection phase before its transition into fast reconnection phase [3]. It is found that the formation of microscopic current sheets (CSs) is a necessary condition for the transition from slow collisional reconnection to fast collisionless reconnection [3–5]. The idea that (whistler)wave can catalyze fast reconnection has been explored both theoretically [6–8] and experimentally [9]. It has been found by Drake et al. [6] that a thin CS can be broken into small scale vortices by whistler wave turbulence and hence facilitate the fast reconnection. They also showed that prior to breakup of the CS, the critical thickness of the CS is smaller than the electron skin depth. Generation of fractal CS structure is also thought to be a way that links the microscopic and macroscopic scales in reconnection [10]. One approach to induce a fractal CS is via a series of macroscopic MHD instabilities, such as secondary tearing mode, Rayleigh-Taylor instability [11], etc. It is a "top-down" process, cascading from macro-scales to micro-scales. Another approach is a "bottom-up" process, i.e., formation of the fractal CS is initiated via microscopic instabilities. This process is plausible when the thickness of the CS shrinks into a very thin level (e.g., a hybrid width of ion skin depth and electron skin depth). By then, microscopic instabilities (e.g., streaming instability, whistler wave, etc.) tends to be excited. In this paper, we study the precursor of the fast reconnection, where the nonlinearity is weak and hence a perturbation analysis is applicable. By investigating the dynamics of the CS prior to the fast reconnection, we give an estimation of a possible process of the interaction of electron- and ion-beam-driven instabilities during their passage through a CS.

The onset of fast reconnection usually happens in a violent way, which is quite analogous to critical-phase-transition phenomena. In general critical phenomena, the state of the system is measured by its order parameter. As the system approaches to its critical point of phase transition, the order parameter undergoes a sudden increase, so that the system evolves into a new state. For the evolution of a CS, the amplitude of the current density disturbance is a natural order parameter. In laminar reconnection scenario, the amplitude of the disturbance is small. Once the phase transition occurs, the order parameter will acquire a finite amplitude transiently. So that the CS becomes rough, which tends to facilitate the formation of fractal CS structure, and hence the fast reconnection is induced. The normal formalism, describing critical-phase-transition/subcritical bifurcation, is Landau-Ginsburg theory [12]. For a narrow CS, the two typical microscopic modes are streaming instability and and whistler mode, which are driven by the strength of current intensity and the gradient of current density, respectively. *An caveat:* for "narrow," we mean a CS with a thickness between ion skin depth and electron skin depth, thus both the ions' and electrons' dynamics should be incorporated. As a paradigmatic model, we choose current-driven-ion-acoustic (CDIA) as the representative of the streaming mode. The CDIA is an electrostatic mode, and it occurs when electron temperature is much higher than ion temperature [13]. The current gradient driven whistler wave (CGDW) is an electromagnetic mode and has been observed experimentally in the electron diffusion regime [14, 15]. We find that, under the joint interactions of CDIA and CGDW, the CS evolution is governed by a Landau-Ginsburg type equation. Once the CS is narrower than a critical thickness, the order parameter of the CS will acquire a finite value via subcritical bifurcation, and then the CS evolve into a rough state (but keep its topology). The roughened CS can be easily broken up by various instabilities, e.g., micro-tearing mode, KH mode [6], and hence accelerate the corresponding magnetic reconnection. We also make an estimation of the critical thickness of the CS, which is about $10d_e$ and is larger than that in Drake et al. [6]. The physics picture discussed in this paper is consistent with the results given by other approaches [6, 16].

The rest of the paper is organized as follows. In Section 2, the linear dynamics of CDIA and CGDW is analyzed. Section 3 gives a heuristic discussion of the nonlinear dynamics of CDIA and CGDW. Combining the conclusions in Sections 2 and 3, a Landau-Ginsburg evolution equation for the current density disturbance is obtained, and its bifurcation property is discussed in Section 4. Section 5 is a summary.

2. Linear Dynamics of CDIA and CGDW

Since electrons are the primary carriers of the current density, for simplicity, we assume the CS being purely composed of electrons, and hence all the free energy of the CS is stored in the electrons current sheet. The evolution of the electron distribution function is

$$\frac{\partial}{\partial t}f_e + \vec{v}_e \cdot \frac{\partial}{\partial \vec{x}}f_e + (-\frac{e\vec{E}}{m_e} - e\vec{v} \times \vec{B}) \cdot \frac{\partial}{\partial \vec{v}_e}f_e = 0 \qquad (1)$$

where the collision effect in neglected. Integrating Equation (1) over $\vec{v}_{e,\perp}$($\perp$ means perpendicular to the guide field in $\hat{z}$) yields a drift-kinetic equation

$$\frac{\partial}{\partial t}F_e + v_{e,z}\frac{\partial}{\partial z}F_e - \frac{eE_z}{m_e} \cdot \frac{\partial}{\partial v_{e,z}}F_e + V_{e,\perp} \cdot \frac{\partial}{\partial \vec{x}_\perp}F_e = 0, \qquad (2)$$

where $F_e = \int f_e d\vec{v}_{e,\perp}$ and $\vec{V}_{e,\perp} = \int \vec{v}_{e,\perp} f_e d\vec{v}_{e,\perp}$. In Equation (2), the parallel and perpendicular kinetic of F_e are linearly coupled, so evolution of F_e can be decomposed into the following two processes

$$\frac{\partial}{\partial t}F_e|_\parallel = -v_{e,z}\frac{\partial}{\partial z}F_e + \frac{eE_z}{m_e} \cdot \frac{\partial}{\partial v_{e,z}}F_e, \qquad (3)$$

and

$$\frac{\partial}{\partial t}F_e|_\perp = -V_{e,\perp} \cdot \frac{\partial}{\partial \vec{x}_\perp}F_e. \qquad (4)$$

For the parallel kinetics, the evolution of the CS is driven by the free energy stored in the strength of the current intensity. A simplest, nontrivial choice for the relevant mode is CDIA, which transfers the momentum of electrons to that of ions [17]. The perpendicular kinetics is determined by the evolution of the perpendicular collective velocity $V_{e,\perp}$, which is in turn determined by the EMHD equation. Therefore, the relevant mode to perpendicular dynamics of the CS is CGDW, which is driven by the free energy stored in the spatial gradient of the CS and is a whistler-like instability and is related to electron momentum transport [18, 19]. A consistent and complete treatment of the CS dynamics must deal with these two modes, simultaneously. Under the driving of inflow, the CS shrinks to a thin layer, and both the strength and the inhomogeneity of the current density tends to increase, so that both CDIA and CGDW modes may appear. *An caveat:* the realistic motions of particles inside a CS are extreme complex [16] and could invalid the use of drift-kinetic equation. However, the full kinetic 3D simulations indeed observed efficient particle acceleration inside a reconnecting CS and hence streaming instabilities (e.g., two electron beam instability) tend to occur inside a CS [16]. In the purpose of having a general view (not going the details of full kinetics of particles) of interaction between particle beams, we employ the drift-kinetic equation.

Since the CDIA and CGDW have been extensive studied in literatures [18–21], we provide a brief and heuristic discussion of the linear and nonlinear features of the CDIA and the CGDW modes, and focus on the evolution of the CS under the physics consequence of the joint interactions of these two modes.

2.1. Linear Instability of CDIA

CDIA belongs to a kind of electron streaming mode, which serves to generate anomalous resistivity. The CDIA occurs when the electron temperature, T_e, significantly exceeds the ion temperature, T_i, e.g., in flare environment [20, 22]. Or else, it will be strongly suppressed by the ion Landau damping. Nevertheless, if $T_e \simeq T_i$, a different streaming instability, Buneman instability, might occur, which has a higher velocity threshold in the order of electron thermal velocity, v_{the}. CDIA and Buneman instabilities only differ in details, and they share the common physical basis of a streaming instability triggered by electron streaming velocity that exceed critical values [13]. In fact, it leads to a similar conclusion if we replace the CDIA with Buneman instability.

The initial current sheet is assumed in a laminar state. The maximum of current density is at the mid-plane ($x = 0$) of the CS, and decays to zero at the edge in a *linear* way (**Figure 1**). (x, y) is the reconnection plane with $\pm\hat{y}$ the direction of outflows. A strong guide field is in the out-of-plane direction, so the lower hybrid drift instability is excluded in the present paper [23]. We choose this profile for simplicity and a more realistic CS configuration can be chosen, but it is expected that the qualitative conclusion will not change. CDIA is well studied in literatures [17, 21, 24], so we directly write its dispersion relation as follows

$$\omega_k^{CDIA} = k_z v_c, \tag{5}$$

$$\gamma_k^{CDIA} = \frac{\pi}{2}|\omega_k^{CDIA}|\left(\langle v_e\rangle - v_c\right)\bar{f}_e\left(\frac{\omega_k^{CDIA}}{k_z}\right), \tag{6}$$

where ω_k^{CDIA} is the real frequency and γ_k^{CDIA} is the linear growth rate of the CDIA. k_z is the wavenumber in z direction, $\langle v_e\rangle$ is the mean electron streaming velocity in $\hat{z}$, and v_c is the threshold velocity. Neglecting the effect of a mean electric field, which is small in the precursor of fast reconnection, v_c is just the ion acoustic speed. Though a mean electric field may slightly shift the value of the threshold velocity [21], the structures of the dispersion relations, Equations (5) and (6), will not change. In the Appendix, we present a derivation of γ_k^{CDIA} in the existence of a weak mean electric field, and show that only is the threshold velocity slightly shifted. As an illustration, we use the results of Bychenkov et al. [21]:

$$v_c = ac_s, \tag{7}$$

where $c_s = (T_i + T_e/m_i)^{1/2}$ is the ion acoustic speed, m_i is the ion mass, and $a = 2.14$. The equilibrium distribution function of electrons is

$$\bar{f}_e(v_z) = \frac{1}{\sqrt{\pi}\, v_{the}} e^{-\frac{(v_z - \langle v_e\rangle)^2}{v_{the}^2}}.$$

Without losing of generality, the electron streaming velocity at the center of the CS is taken to be marginal, i.e., $\langle v_e\rangle(x = 0) = v_c$. We also assume $\langle v_e\rangle(x)$ varying linearly, $\langle v_e\rangle(x) = v_c + \langle v_e\rangle' x$, with current shear $\langle v_e\rangle' < 0$ (here we take $x > 0$). Then the general form of $\gamma_k^{CDIA}(x)$ for a inhomogeneous CS follows as

$$\gamma_k^{CDIA} \simeq \frac{\sqrt{\pi}}{2}\frac{|\omega_k^{CDIA}|\,\langle v_e\rangle'}{v_{the}}x, \tag{8}$$

where $\bar{f}_e\left(\frac{\omega_k^{CDIA}}{k_z}\right) = \bar{f}_e(v_c) \simeq \frac{1}{\sqrt{\pi}v_{the}}$. γ_k^{CDIA} has been assumed to be marginal in the middle plane of the CS, it becomes more and more negative as approaching the edge.

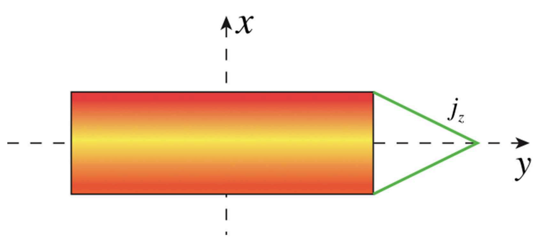

FIGURE 1 | Sketch of the initial configuration of the CS.

2.2. Linear Instability of CGDW

CGDW is an electromagnetic mode and can be described by EMHD equation [25]

$$\frac{\partial}{\partial t}\mathbf{B} + d_e^2\frac{\partial}{\partial t}\nabla \times \mathbf{j}_e = -d_e^2\nabla \times \left(\mathbf{v}_e \cdot \nabla\mathbf{j}_e - d_e^{-2}\mathbf{v}_e \times \mathbf{B}\right), \tag{9}$$

where d_e is the electron skin depth, $j_e = -en_e v_e = \nabla \times B$ is the electron current density, and B is the total magnetic field with a strong guide component in $\hat{z}$. The linear growth rate of the CGDW is proportional to the gradient of the CS. By extracting the free energy terms in linearizing Equation (9), one has

$$\begin{aligned} &\tfrac{\partial}{\partial t}\tilde{\mathbf{B}} + d_e^2\tfrac{\partial}{\partial t}\nabla \times \tilde{\mathbf{j}}_e = \\ &-d_e^2\left(\langle j_e\rangle'\nabla\tilde{v}_{ex} \times \hat{z} + \nabla\langle v_e\rangle \times \partial_z\tilde{\mathbf{j}}_e\right) - \langle v_e\rangle'\tilde{B}_x\hat{z}, \end{aligned} \tag{10}$$

where the terms with higher spatial derivatives($\langle v_e\rangle,'' \langle v_e\rangle'''$...) are ignored. Employing the transformations of $\partial_t \to \gamma_k^{CGDW}$, $\nabla \to ik$ yields

$$\begin{aligned} &\gamma_k^{CGDW}\left(1 + k^2d_e^2\right)\tilde{\mathbf{B}} = \\ &-d_e^2\left(i\langle j_e\rangle'\tilde{v}_{ex}\mathbf{k} \times \hat{z} + ik_z\langle v_e\rangle'\hat{x} \times \tilde{\mathbf{j}}_e\right) - \langle v_e\rangle'\tilde{B}_x\hat{z}. \end{aligned} \tag{11}$$

γ_k^{CGDW} is solved as

$$\gamma_k^{CGDW} = \frac{|k_y|d_e}{1 + k^2d_e^2}|\langle v_e\rangle'|, \tag{12}$$

In the above derivation, we have assumed that the current density shear is caused by electron drift velocity, other than density inhomogeneity [26, 27].

Though CGDW is driven by gradient of current density, it is not electron Kelvin-Helmholtz (KH) mode. The real frequency of CGDW is in the order of the whistler frequency, while the electron KH mode is a purely growing mode. CGDW is driven predominantly by the gradient in the out-of-plane current density, while electron KH mode is driven by shears of the in-plane electron flows [9, 28, 29]. Therefore, CGDW and electron KH modes are two different types of instabilities. Whistler wave has been confirmed in laboratory experiments and satellite observations, and is considered to be important in initiating fast reconnection [6, 14, 15]. In simulations, a current gradient driven mode with similar features has also been observed [30].

3. Nonlinear Dynamics of CDIA and CGDW Modes

Prior to the onset of fast reconnection, the nonlinearities of the parallel and perpendicular dynamics are weak, so that a perturbation analysis of the nonlinear dynamics of the CS is applicable.

3.1. Nonlinear Instability of CDIA

To the first order, $\bar{f}_e$ is adiabatically shifted [31] by a *finite* perturbation of electron drift velocity in $\hat{z}$ (See **Figure 2**), $\tilde{v}_{e,z}$, i.e.,

$$\bar{f}_e(v_z) \rightarrow \frac{1}{\sqrt{\pi} v_{the}} e^{-\frac{(v_z-\langle v_e\rangle-\tilde{v}_{e,z})}{v_{the}^2}}. \quad (13)$$

Depending on the sign of $\tilde{v}_{e,z}$, the nonlinear change of the free energy in the intensity of the current density is positive ($\tilde{v}_e > 0$, the red one in **Figure 2**) or negative ($\tilde{v}_{e,z} < 0$, the blue one in **Figure 2**). For the positive change, the CDIA is nonlinearly unstable, or else it is nonlinearly stable. Substituting Equation (13) into Equation (6), the nonlinear growth rate is readily derived as

$$\gamma_{NL}^{CDIA} = \frac{\pi}{2}|\omega_k^{CDIA}|\tilde{v}_{e,z}\bar{f}_e\left(\frac{\omega_k^{CDIA}}{k_z}\right) \simeq \alpha_k \tilde{v}_{e,z}, \quad (14)$$

where $\alpha_k = \frac{\sqrt{\pi}}{2}|\omega_k^{CDIA}|/v_{the}$.

Combining Equations (8) and (14), the evolution of $|\tilde{v}_{e,z}|$ driven by CDIA is (i.e., Equation 3)

$$\left(\frac{\partial}{\partial t}|\tilde{v}_{e,z}|\right)_{CDIA} \simeq \gamma_{CDIA}|\tilde{v}_{e,z}| + \alpha\tilde{v}_{e,z}|\tilde{v}_{e,z}|, \quad (15)$$

where $\gamma_{CDIA} = \sum_k \gamma_k^{CDIA}$ and $\alpha = \sum_k \alpha_k$. $\sum_k \alpha_k \tilde{v}_{ez,k} \simeq \alpha\tilde{v}_{e,z}$ is used in deriving Equation (15), because the spectrum width of CDIA modes is narrow in the initial nonlinear stage. For a positive perturbation (the case of interest), the CS is nonlinearly unstable and hence, to reach a saturated state, one needs consider higher order nonlinear interaction. For acoustic turbulence [32], three-wave coupling is lacked, and the next-to-order nonlinear interaction scales as $O(|\tilde{v}_{e,z}|^3)$. Therefore, for the nonlinear dynamics of CDIA, only the lowest nonlinear interaction needs to be included.

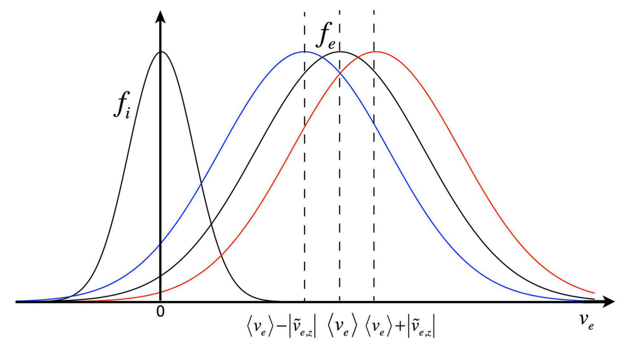

FIGURE 2 | Sketch of nonlinear shift of $\bar{f}_e$.

3.2. Nonlinear Dynamics of CGDW

It has been demonstrated that a sharpening CS can be flattened via a (nonlinear)hyper-diffusion [33, 34], which corresponds to the electron momentum transport perpendicular to the CS. There are also accumulated numerical evidence that point to the plausibility of a hyper-diffusion process in broadening the CS [18]. Here we focus on the general structure of the current density evolution equation in the impact of the CGDW turbulence. The nonlinearity of Equation (9) comes from the two terms on the RHS of Equation (9). Since both $\tilde{v}_e$ and $\tilde{B}$ are functions of $\tilde{j}$, the strength of the nonlinear interaction of Equation (9) is $\sim j^2$. Keeping minimal algebras, we write the nonlinear evolution of a "test" mode ($\tilde{j}_{z,k}$) as

$$\left(\frac{\partial}{\partial t}\tilde{j}_{z,k}\right)_{nl} = \sum_{k'} C(k,k')\tilde{j}_{z,-k'}\tilde{j}_{z,k'+k}, \quad (16)$$

where $C(k,k')$ is the nonlinear coupling coefficient given by Equation (9). The three components of $\tilde{\mathbf{j}}_k$ are related with each other via Equation (9) and incompressibility condition, $\nabla\cdot\tilde{\mathbf{j}} = 0$. So, the nonlinear coupling on the RHS of Equation (16) can be expressed in the form of self-coupling of $\tilde{j}_{z,k}$. With direct interaction approximation [35], the nonlinear coupling in Equation (16) is approximated as $\tilde{j}_{z,-k'}\tilde{j}_{z,k'+k} \simeq \tilde{j}_{z,-k'}\tilde{j}^{(2)}_{z,k'+k}$, and the coherent response $\tilde{j}^{(2)}_{z,k'+k}$ is given by Equations (9) and (16):

$$\tilde{j}^{(2)}_{z,k'+k} = R_{\omega_{k'+k},k'+k}C(k,k')\tilde{j}_{z,-k'}\tilde{j}_{z,k}, \quad (17)$$

where the response function $R_{\omega_{k'+k},k'+k}$ takes the form of

$$R_{\omega_{k'+k},k'+k} = \frac{1}{-i\left(\omega_{k'+k} - \omega_{whistler} - (k_z+k'_z)\langle v_e\rangle\right) + \gamma_{k'+k}^{CGDW}}. \quad (18)$$

Here $\omega_{whistler}$ is the whistler frequency, and $(k_z+k'_z)\langle v_e\rangle$ is the effect of Doppler shift. In the resonance condition $\omega_{k'+k} - \omega_{histler} - (k_z+k'_z)\langle v_e\rangle = 0$), $R_{\omega_{k'+k},k'+k}$ is simplified as

$$R_{\omega_{k'+k},k'+k} = \frac{1}{\gamma_{k'+k}^{CGDW}} \quad (19)$$

Combining Equations (17) and (19), Equation (16) yields

$$\left(\frac{\partial}{\partial t}\tilde{j}_{z,k}\right)_{nl} \simeq \sum_{k'} \frac{C(k,k')}{\gamma_{k+k'}^{CGDW}}\left|\tilde{j}_{z,k'}\right|^2\tilde{j}_z. \quad (20)$$

Since the spectrum of $\tilde{j}_{z,k}$ is narrow, one has $\tilde{j}_{z,k'} \simeq \tilde{j}_{z,k}$. Equation (20) is further approximated as

$$\left(\frac{\partial}{\partial t}\tilde{j}_{z,k}\right)_{nl} \simeq -\beta_k\left|\tilde{j}_{z,k}\right|^2\tilde{j}_{z,k}, \quad (21)$$

where

$$\beta_k = -\sum_{k'} \frac{C(k,k')}{\gamma^{CGDW}_{k+k'}}.$$

The "test" mode $\tilde{j}_{z,k}$ is stabilized by the nonlinear term in Equation (21), so β_k should be a *positive* coupling coefficient [36]. Combining Equations (12) and (21), one obtains the evolution of $|\tilde{v}_{e,z}|$ driven by CGDW (i.e., Equation 4)

$$\left(\frac{\partial}{\partial t}|\tilde{v}_{e,z}|\right)_{CGDW} \simeq \gamma_{CGDW}|\tilde{v}_{e,z}| - \beta|\tilde{v}_{e,z}|^3, \tag{22}$$

where $\gamma_{CGDW} = \sum_k \gamma_k^{CGDW}$ and $\sum_k \beta_k \left|\tilde{j}_{z,k}\right|^2 \tilde{j}_{z,k} \simeq \beta|\tilde{v}_{e,z}|^3$ with $\beta = \sum_k \beta_k (en_0)^3 > 0$.

4. Subcritical Bifurcation of the CS

Combining Equations (15) and (22) yields the full evolution equation of $|\tilde{v}_{e,z}|$

$$\frac{\partial}{\partial t}|\tilde{v}_{e,z}| = \gamma_L|\tilde{v}_{e,z}| + \alpha\tilde{v}_{e,z}|\tilde{v}_{e,z}| - \beta|\tilde{v}_{e,z}|^3, \tag{23}$$

where the total linear growth rate γ_L is

$$\begin{aligned}\gamma_L &= \gamma_{CDIA} + \gamma_{CGDW} \\ &= \sum_k \frac{\sqrt{\pi}v_c}{2v_{the}}|k_z|\,(x_c - x)\,|\langle v_e\rangle'|,\end{aligned} \tag{24}$$

and its marginally stable position is

$$x_c = \frac{2}{\sqrt{\pi}}\frac{d_e}{1+k^2d_e^2}\left|\frac{k_y}{k_z}\right|\left|\frac{v_{the}}{v_c}\right|. \tag{25}$$

Since the edge of the CS is relatively the most stable point, we take it as an indicator of the global state of the CS. In other words, if phase transition occurs at the edge, the whole CS will transit into the new state, too. The bifurcation property of Equation (23) is determined by the sign of $\tilde{v}_{e,z}$. For a positive perturbation, $\tilde{v}_{e,z} > 0$, the CS is *subcritical* bifurcation, or else it is *supercritical* bifurcation. In the supercritical bifurcation case, both the nonlinear terms tend to stabilize the linear term, so that the amplitude of the order parameter is constrained to a relative small value. While in the subcritical bifurcation case, the first nonlinear interaction on the RHS of Equation (23) is nonlinearly unstable, so that $\tilde{v}_{e,z}$ can acquire an *finite* value after the phase transition. Therefore, the subcritical bifurcation is more relevant to the onset of fast magnetic reconnection, and it is the case of interest in the present paper.

In the subcritical bifurcation scenario, $\tilde{v}_{e,z} = |\tilde{v}_{e,z}|$ and Equation (23) becomes

$$\frac{\partial}{\partial t}|\tilde{v}_{e,z}| = \gamma_L|\tilde{v}_{e,z}| + \alpha|\tilde{v}_{e,z}|^2 - \beta|\tilde{v}_{e,z}|^3, \tag{26}$$

which is a real *Landau-Ginzburg* equation [12]. The corresponding free energy is

$$F\left(|\tilde{v}_{e,z}|\right) = -\frac{\gamma_L}{2}|\tilde{v}_{e,z}|^2 - \frac{\alpha}{3}|\tilde{v}_{e,z}|^3 + \frac{\beta}{4}|\tilde{v}_{e,z}|^4 \tag{27}$$

In the steady state, one has $\delta F/\delta|\tilde{v}_{e,z}| = 0$. $|\tilde{v}_{e,z}|$ is solved as

$$|\tilde{v}_{e,z}|_I = \frac{\alpha + \sqrt{\alpha^2 + 4\beta\gamma_L}}{2\beta}, \qquad x \geq 0 \tag{28}$$

$$|\tilde{v}_{e,z}|_{II} = \frac{\alpha - \sqrt{\alpha^2 + 4\beta\gamma_L}}{2\beta}, \qquad x \geq x_c \tag{29}$$

$$|\tilde{v}_{e,z}|_{III} = 0. \qquad x \geq 0 \tag{30}$$

Figure 3 provides a schematic illustration of the three types of solutions and their stabilities.

The most remarkable feature of these solutions is their subcritical bifurcation. At the beginning, the nonlinearity (the 2nd term on the RHS of Equation 26) of the CDIA starts to drive the current density perturbation (i.e., $\tilde{v}_{e,z}$) to grow in an explosive way. Transiently, the hyper-diffusion induced by the nonlinearity (the 3rd term on the RHS of Equation 26) of the CGDW comes into effect and saturates the explosive growth. Via the above process, the order parameter acquires a finite value instantly and the CS evolves into a rough state.

The subcritical bifurcation occurs at

$$\begin{aligned}x_b &= \frac{\sum_k |k_z|x_c}{\sum_k |k_z|} + \frac{\alpha}{4\beta} \\ &\simeq x_c + \frac{\sqrt{\pi}v_c}{8v_{the}}\overline{C}\sum_k \frac{|k_z|}{|k_y|}\frac{(1+k^2d_e^2)}{d_e|\langle v_e\rangle'|},\end{aligned} \tag{31}$$

with $\overline{C} = -\sum_{k,k'} C\left(k,k'\right)(en_0)^3$. The 2nd term on the RHS of Equation (31) scales as $\sim (m_e/m_i)^{1/2}d_e$. Compared with $x_c(\sim (m_i/m_e)^{1/2}d_e)$, it is negligible. For isotropic turbulence, substituting Equation (7) into Equation (25) yields the critical thickness of the CS,

$$\begin{aligned}\Delta_c \simeq 2x_c \simeq \frac{2}{a\sqrt{\pi}}\left(\frac{T_e}{T_i+T_e}\right)^{1/2}\left(\frac{m_i}{m_e}\right)^{1/2} \\ \frac{d_e}{1+k^2d_e^2} \sim \frac{10}{1+k^2d_e^2}d_e,\end{aligned} \tag{32}$$

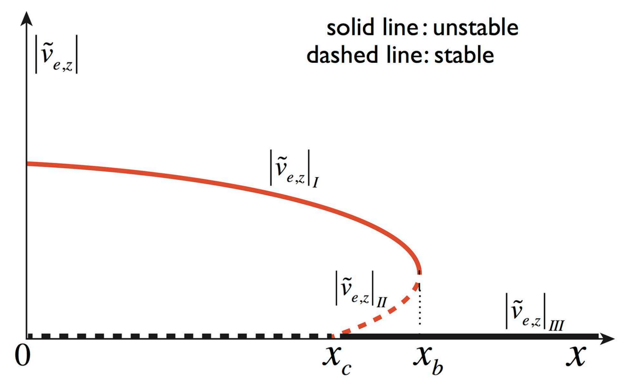

FIGURE 3 | Bifurcation diagram: solid lines represent unstable points, and dashed lines represent stable points. The red lines represents the solutions, $|\tilde{v}_{e,z}|_I$ and $|\tilde{v}_{e,z}|_{II}$, and black line represents the solution, $|\tilde{v}_{e,z}|_{III}$.

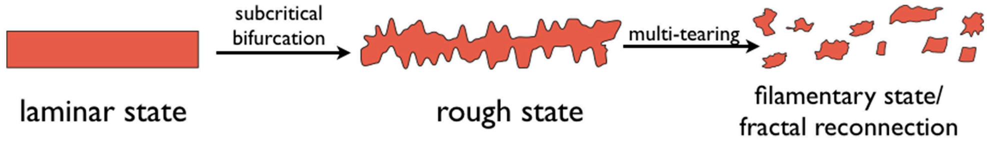

FIGURE 4 | Sketch of the formation of rough CS and the following filamentation.

where $T_e \gg T_i$ is used and $d_e < |k^{-1}| < d_i$. Equation (32) indicates that the mass ratio of ion and electron plays an important role in determining the critical thickness [37]. The above crude estimation is also comparable with experimental observations [37, 38]. As is pointed out earlier, the specific value of the critical thickness is very sensitive to the type of streaming instability. For example, if the streaming instability is Buneman instability, which has a much higher threshold velocity in the order of electron thermal velocity [13], putting $v_c \simeq v_{the}$ into Equation (25), the corresponding critical thickness is approximately $\Delta_c \sim d_e$. It should be pointed out that the proceeded calculation can only give a simple estimation. For more precise and complete description of the CS dynamics, first principle 3D simulations are needed [16].

The phase transition of the CS proceeds in an explosive way. We can see this by observing the temporal behavior of $|\tilde{v}_{e,z}|$. In the early nonlinear stage, the 1st and 3rd terms on the RHS of Equation (26) are ignorable, and one has

$$\frac{\partial}{\partial t}|\tilde{v}_{e,z}| \simeq \alpha |\tilde{v}_{e,z}|^2. \tag{33}$$

Thus, $|\tilde{v}_{e,z}|$ scales as $|\tilde{v}_{e,z}| \sim (t_0 - t)^{-1}$ and time t_0 is determined by initial conditions. Near the phase transition point, the CS grows so fast that other instabilities (e.g., tearing mode) have no time to make a significant impact on the transition process. Under the driving of the inflow, the CS shrinks along the stable line (state $|\tilde{v}_{e,z}|_{III}$, solid, black line in **Figure 3**) to a thickness equaling to Δ_c, and then it subcritically bifurcates into the state, $|\tilde{v}_{e,z}|_I$, where the order parameter $|\tilde{v}_{e,z}|$ acquires a *finite* value, instantly. Consequently, the CS is deformed and becomes rough, but its topology is not changed. The newly induced rough structures will facilitate the occurrence of micro-instabilities, e.g., micro-tearing mode, and hence induce fast reconnection. **Figure 4** provides a diagrammatic sketch of this process.

5. Summary

In this paper, we study the nonlinear dynamics of a CS prior to the onset of fat reconnection. We show that under the joint interactions of the CDIA and CGDW, the CS can transmit into a rough state from a laminar state via subcritical bifurcation. The thickness of the CS is a "controller" of the phase transition. The phase transition occurs once it is narrower than a critical value. The rough CS can facilitate the formation of a fractal CS, and hence induce fast reconnection. Through the critical thickness is predicted as $\Delta_c \sim 10d_e/(1 + k^2 d_e^2)$, the model proposed here is only paradigmatic. As we stressed in the paper, the type of streaming instability is very important in giving a quantitative prediction of Δ_c. Also, in this work we focus on the CS dynamics below the ion skin depth, and the kinetic effect [e.g., kinetic Alfvén wave (KAW)] of ions is ignored [39, 40]. In the KAW dominant regime (characteristic scale of fluctuations is order of ion's skin depth/Lamor radius), the nonlinear dynamics of the CS will be determined by the joint interactions of streaming instability and KAW instability. However, since the dispersion relation of whistler wave and KAW are similar, it can expect that the CS will also undergo subcritical bifurcation process at some other critical width. The qualitative physics picture proposed in this paper is testable in numerical studies dedicated to the onset of fast reconnection [41].

Acknowledgments

This work was supported by the Ministry of Science and Technology of China under Grant Nos. 2013GB111001, and 2013GB112002. ZG was also supported by the WCI Program of the National Research Foundation of Korea funded by the Ministry of Education, Science and Technology of Korea [WCI 2009-001].

References

1. Walsh AP, Fazakerley AN, Lahiff AD, Volwerk M, Grocott A, Dunlop MW, et al. Cluster and double star multipoint observations of a plasma bubble. *Ann Geophys.* (2009) **27**:725–43. doi: 10.5194/angeo-27-725-2009
2. Owen CJ, Marchaudon A, Dunlop MW, Fazakerley AN, Bosqued JM, Dewhurst JP, et al. Cluster observations of crater flux transfer events at the dayside high-latitude magnetopause. *J Geophys Res.* (2008) **113**:A07504. doi: 10.1029/2007JA012701
3. Cassak P, Shay M. Magnetic reconnection for coronal conditions: reconnection rates, secondary islands and onset. *Space Sci Rev.* (2012) **172**:283–302. doi: 10.1007/s11214-011-9755-2
4. Daughton W, Scudder J, Karimabadi H. Fully kinetic simulations of undriven magnetic reconnection with open boundary conditions. *Phys Plasmas.* (2006) **13**:072101. doi: 10.1063/1.2218817
5. Daughton W, Roytershteyn V. Emerging parameter space map of magnetic reconnection in collisional and kinetic regimes. *Space Sci Rev.* (2011) **172**:271. doi: 10.1007/s11214-011-9766-z

6. Drake JF, Biskamp D, Zeiler A. Breakup of the electron current layer during 3-D collisionless magnetic reconnection. *Geophys Res Lett*. (1997) **24**: 2921–4. doi: 10.1029/97GL52961
7. Shay MA, Drake JF, Denton RE, and, Biskamp D. Structure of the dissipation region during collisionless magnetic reconnection. *J Geophys Res Space Phys*. (1998) **103**:9165–76. doi: 10.1029/97JA03528
8. Shay MA, Drake JF, Rogers BN, and Denton RE. The scaling of collisionless, magnetic reconnection for large systems. *Geophys Res Lett*. (1999) **26**: 2163–6. doi: 10.1029/1999GL900481
9. Deng XH, Matsumoto H. Rapid magnetic reconnection in the Earth's magnetosphere mediated by whistler waves. *Nature* (2001) **410**:557–60. doi: 10.1038/35069018
10. Tajima T, Shibata K. *Plasma Astrophysics*. Massachusetts: Addison-Wesley (1997).
11. Isobe H, Shibata K. Reconnection in solar flares: outstanding questions. *J Astrophys Astr*. (2009) **30**:79–85. doi: 10.1007/s12036-009-0007-8
12. Crawford JD. Introduction to bifurcation theory. *Rev Mod Phys*. (1991) **63**:991. doi: 10.1103/RevModPhys.63.991
13. Roussev I, Galsgaard K, Judge PG. Physical consequences of the inclusion of anomalous resistivity in the dynamics of 2D magnetic reconnection. *Astron Astrophys*. (2002)**382**:639–49. doi: 10.1051/0004-6361:20011645
14. Ji H, Terry S, Yamada M, Kulsrud R, Kuritsyn A, Ren Y. Electromagnetic fluctuations during fast reconnection in a laboratory plasma. *Phys Rev Lett*. (2004) **92**:115001. doi: 10.1103/PhysRevLett.92.115001
15. Singh N. Whistler mode based explanation for the fast reconnection rate measured in the MIT versatile toroidal facility. *Phys Rev Lett*. (2011) **107**:245003. doi: 10.1103/PhysRevLett.107.245003
16. Siversky TV, Zharkova VV. Particle acceleration in a reconnecting current sheet: PIC simulation. *J Plasma Phys*. (2009) **75**:619–36. doi: 10.1017/S0022377809008009
17. Sagdeev RZ. On Ohms law resulting from instability. *Proc Symp Appl Math*. (1967) **18**:281. doi: 10.1090/psapm/018/9919
18. Drake JF, Kleva RG, Mandt ME. Structure of thin current layers: implications for magnetic reconnection. *Phys Rev Lett*. (1994) **73**:1251. doi: 10.1103/PhysRevLett.73.1251
19. Che H, Drake JF, Swisdak M. A current filamentation mechanism for breaking magnetic field lines during reconnection. *Nature* (2011) **474**:184–7. doi: 10.1038/nature10091
20. Uzdensky DA. Petschek-like reconnection with current-driven anomalous resistivity and its application to solar flares. *Astrophys J*. (2003) **587**:450–7. doi: 10.1086/368075
21. Bychenkov VY, Silin VP, Uryupin SA. Ion-acoustic turbulence and anomalous transport. *Phys Rep*. (1988) **164**:119–215. doi: 10.1016/0370-1573(90)90122-I
22. Rosner R, Golub L, Coppi B, Vaiana GS. Heating of coronal plasma by anomalous current dissipation. *Astrophys J*. (1978) **222**:317. doi: 10.1086/156145
23. Davidson RC, Gladd NT, Wu CS, Huba JD. Effects of finite plasma beta on the lower-hybrid-drift instability. *Phys Fluids*. (1977) **20**:301. doi: 10.1063/1.861867
24. Diamond PH, Itoh S-I, Itoh K. *Modern Plasma Physics: Physical Kinetics of Turbulent Plasmas,* Vol. 1. Cambridge, UK: Cambridge University Press (2010).
25. Priest E, Forbes T. *Magnetic Reconnection: MHD Theory and Applications.* Cambridge, UK: Cambridge University Press (2007).
26. Asano Y, Nakamura R, Baumjohann W, Runov A, Vörös Z, Volwerk M, et al. How typical are atypical current sheets? *Geophys Res Lett*. (2005) **32**:108. doi: 10.1029/2004GL021834
27. Zelenyi LM, Malova HV, Artemyev AV, Popovc VY, Petrukovich AA. Thin current sheets in collisionless plasma: equilibrium structure, plasma instabilities, and particle acceleration. *Plasma Phys Rep*. (2011) **37**: 118–60. doi: 10.1134/S1063780X1102005X
28. Ferraro, NM Rogers BN. Turbulence in low-beta reconnection. *Phys Plasmas*. (2004) **11**:4382. doi: 10.1063/1.1776565
29. Loureiro NF, Schekochihin AA, Uzdensky DA. Plasmoid and kelvin-helmholtz instabilities in sweet-parker current sheets. *Phys Rev E*. (2013) **87**:013102. doi: 10.1103/PhysRevE.87.013102
30. Fujimoto K, Sydora RD. Plasmoid-induced turbulence in collisionless magnetic reconnection. *Phys Rev Lett*. (2012) 109:265004. doi: 10.1103/PhysRevLett.109.265004
31. Rosenbluth MN, Dagazian RY, Rutherford PH. Nonlinear properties of the internal m= 1 kink instability in the cylindrical tokamak. *Phys Fluids*. (1973) **16**:1894–902. doi: 10.1063/1.1694231
32. Zakharov VE, Sagdeev RZ. Spectrum of acoustic turbulence. *Sov Phys Dokl*. (1970) **15**:439.
33. Boozer AH. Ohm's law for mean magnetic fields. *J Plasma Phys*. (1986) **35**:133. doi: 10.1017/S0022377800011181
34. Bhattacharjee A, Hameiri E. Self-consistent dynamolike activity in turbulent plasmas. *Phys Rev Lett*. (1986) **57**:206. doi: 10.1103/PhysRevLett.57.206
35. Kadomtsev BB. *Plasma Turbulence*. New York, NY: Academic Press (1965).
36. Guo ZB, Diamond PH, Wang XG. Magnetic reconnection, helicity dynamics, and hyper-diffusion. *Astrophys J*. (2012) **757**:173. doi: 10.1088/0004-637X/757/2/173
37. Ren Y, Yamada M, Ji H, Gerhardt SP, Kulsrud R. Identification of the electron-diffusion region during magnetic reconnection in a laboratory plasma. *Phys Rev Lett*. (2008) **101**:085003. doi: 10.1103/PhysRevLett.101.085003
38. Zhong JY, Li YT, Wang XG, Wang JQ, Dong QL, Xiao CJ, et al. Modeling looptop X-ray source and reconnection outflows in solar flares with intense lasers. *Nat Phys* (2010) **6**:984–7. doi: 10.1038/nphys1790
39. Rogers BN, Denton RE, Drake JF, and Shay MA. Role of dispersive waves in collisionless magnetic reconnection. *Phys Rev Lett*. (2001) **87**:195004. doi: 10.1103/PhysRevLett.87.195004
40. Boldyrev S, Horaites K, Xia Q, Perez JC. Toward a theory of astrophysical plasma turbulence at subproton scales *Astrophys J*. (2013) **777**:41. doi: 10.1088/0004-637X/777/1/41
41. Singh N. Evolution of an electron current layer prior to reconnection onset. *Phys Rev Lett*. (2012) **109**:145001. doi: 10.1088/0004-637X/777/1/41

Conflict of Interest Statement: The authors declare that the research was conducted in the absence of any commercial or financial relationships that could be construed as a potential conflict of interest.

Appendix

Linear CDIA instability with a weak mean electric field

Constitutive equations for CDIA with a mean electric field are

$$\frac{\partial}{\partial t}f_e + v_{e,z}\frac{\partial}{\partial z}f_e - \frac{eE}{m_e}\frac{\partial}{\partial v_{e,z}}f_e = 0; \quad (A1)$$

$$\frac{\partial}{\partial t}n_i + \frac{\partial}{\partial z}\left(n_i v_{i,z}\right) = 0; \quad (A2)$$

$$m_i n_i\left(\frac{\partial}{\partial t}v_{i,z} + v_{i,z}\frac{\partial}{\partial z}v_{i,z}\right) = -T_i\frac{\partial}{\partial z}n_i + e n_i E; \quad (A3)$$

Equation (A1) is the 1D kinetic equation for electron. Equations (A2) and (A3) are ion's continuity and momentum equation, separately. In deriving the dispersion relation, we write all quantities into a mean piece and a fluctuation piece, i.e., $f_e = \langle f_e\rangle + \tilde{f}_e$, $n_i = n_{i,0} + \tilde{n}_i$, $v_i = \tilde{v}_i$ and $E = \langle E\rangle + \tilde{E}$.

$\tilde{f}_e$ is composed by a adiabatic part, $\frac{e\tilde{\phi}}{T_e}$, and a non-adiabatic, g. Thus, putting $\tilde{f}_e = \frac{e\tilde{\phi}}{T_e} + g$ into Equation (A1) yields the evolution equation for g

$$\frac{\partial}{\partial t}g + v_{e,z}\frac{\partial}{\partial z}g - \frac{e\langle E\rangle}{m_e}\frac{\partial}{\partial v_{e,z}}g = -\left(\frac{\partial}{\partial t}\frac{e\tilde{\phi}}{T_e} + \langle v_e\rangle\frac{\partial}{\partial z}\frac{e\tilde{\phi}}{T_e}\right)\langle f_e\rangle. \quad (A4)$$

The characteristic equations of Equation (A4) are

$$\frac{\partial}{\partial t}x(t) = v(t); \quad (A5)$$

$$\frac{\partial}{\partial t}v(t) = -\frac{e\langle E\rangle}{m_e}. \quad (A6)$$

And their solutions are

$$x(-t) = -vt - \frac{e\langle E\rangle}{2m_e}t^2 + x; \quad (A7)$$

$$v(-t) = \frac{e\langle E\rangle}{m_e}t + v, \quad (A8)$$

where $x(0) = x$ and $v(0) = v$. Then the Green function of Equation (A4) is obtained as

$$G(\omega_k, k_z) = \int_0^\infty e^{i\left(\omega_k - k_z v_{e,z} - k_z\frac{e\langle E\rangle}{2m_e}t\right)t}dt. \quad (A9)$$

The RHS of Equation (A9) can be seen as Laplace transformation of $exp(-ik_z\frac{e\langle E\rangle}{2m_e}t^2)$, i.e., $G(\omega_k, k_z) = \mathcal{L}\left(exp(-ik_z\frac{e\langle E\rangle}{2m_e}t^2)\right)$.

Using the formula,

$$\begin{aligned}\mathcal{L}\left(e^{-iat^2}\right) &= \mathcal{L}\left(\cos at^2\right) - i\mathcal{L}\left(\sin at^2\right)\\ &= \sqrt{\frac{\pi}{2a}}\left(\frac{1}{2} - S\left(\frac{p}{\sqrt{2\pi a}}\right)\right)\left[\cos\frac{p^2}{4a} - i\sin\frac{p^2}{4a}\right]\\ &-\sqrt{\frac{\pi}{2a}}\left(\frac{1}{2} - C\left(\frac{p}{\sqrt{2\pi a}}\right)\right)\left[\sin\frac{p^2}{4a} + i\cos\frac{p^2}{4a}\right],\end{aligned} \quad (A10)$$

where $p = -i\left(\omega_k - k_z v_{e,z}\right)$, $a = k_z\frac{e\langle E\rangle}{2m_e}$ and $S(p)$, $C(p)$ are *Fresnel* functions, one obtains $G(\omega_k, k)$ in the weak mean field limit, $1 \ll \left|\frac{p}{\sqrt{2\pi a}}\right| = 2m_e\left|\frac{(\omega_k - k_z v_{e,z})^2}{ek_z\langle E\rangle}\right|$,

$$G\left(\omega_k, k\right) = \frac{1}{\omega_k - k_z v_{e,z}}\left[1 + i\frac{ek_z\langle E\rangle}{m_e\left(\omega_k - k_z v_{e,z}\right)^2}\right] \quad (A11)$$

By Equations (A4) and (A11), the Fourier component of g is

$$g_{k,\omega_k} = -\frac{\omega_k - k_z\langle v_z\rangle}{\omega_k - k_z v_z}\left[1 + i\frac{ek_z\langle E\rangle}{m_e\left(\omega_k - k_z v_{e,z}\right)^2}\right]\frac{e\phi_{k,\omega_k}}{T_e}\langle f_e\rangle \quad (A12)$$

If the weak mean electric field tens to zero, $\left|\frac{ek_z\langle E\rangle}{m_e(\omega_k - k_z v_{e,z})}\right| \to 1$, the conventional non-adiabatic response is recovered [17, 24]. Then the total response of electron is

$$\frac{\tilde{n}_e}{n_{e,0}} = \frac{e\tilde{\phi}}{T_e} - \frac{e\tilde{\phi}}{T_e}\left[i\pi\frac{\omega_k - k_z v_{e,z}}{|k|v_{the}}\left(1 - \frac{ek_z\langle E\rangle}{m_e\gamma_k^2}\right)\right] \quad (A13)$$

The response of ions' density is obtained from Equations (A2) and (A3)

$$\frac{\tilde{n}_i}{n_{i,0}} = \frac{k_z^2 c_s^2}{\omega_k^2}\frac{e\tilde{\phi}}{T_e} \quad (A14)$$

Using the quasi-neutrality condition, growth rate γ_k^{CDIA} of the CDIA is obtained as

$$\gamma_k^{CDIA} = \frac{\pi}{2}|\omega_k|(\langle v_e\rangle - c_s)\bar{f}_e - \frac{2ek_z}{\pi m_e|\omega_k|\left(\langle v_e\rangle - c_s\right)\bar{f}_e}\langle E\rangle, \quad (A15)$$

where the critical point($\gamma_k^{CDIA} = 0$) is slightly shifted by the mean electric field, but the basic structure of γ_k^{CDIA} is not changed.